4ICEGE
Thessaloniki-GREECE 2007

4th International Conference on
Earthquake Geotechnical Engineering
June 25-28, 2007
Paper No. 1303

OPTIMIZATION OF SENSOR LOCATION BY STATIC AND DYNAMIC SLOPE STABILITY ANALYSIS

Jaime BOJORQUE [1], Guido DE ROECK[2], and Jan MAERTENS [3]

ABSTRACT

This paper derives the best location of field sensor for landslide monitoring based on static, pseudo-static and dynamic finite element slope stability analysis. Use is made of the finite element technique as not to constrain the analysis by the assumptions required in classical approaches. Numerical techniques in general, easily handle the strain-stress relationship, the non-linear soil behaviour, and complex geometries. The present methodology is implemented in a potential landslide site at km 27 along the Cuenca-Machala highway, Ecuador. This site has a cut slope of about 40 degrees with a length of 130 m and it is 100 m wide, given an approximated landslide volume of 240,000 m^3 with an average depth of 18.5 m. The soils behaviour is represented as elastic-plastic soil material with a Mohr-Coulomb failure criterion for which the soil strength parameters were derived from in-situ and laboratory tests. The changes of static and/or dynamic stresses, geometry and soil properties will cause a variation where the highest displacements are developed. The location of the highest total, vertical and horizontal displacements are used to judge the best location for installing sensors for landslide monitoring. Different scenarios are analyzed to evaluate the effect of introducing remedial measures and different transient conditions. The results of the numerical simulation enabled definition of the most efficient and cost-effective location of the sensors to alert for potential landslides.

Keywords: slope stability, finite element, earthquake, monitoring, Ecuador

INTRODUCTION

In general, due to economic constraints it is not possible to implement a entire network of landslide monitoring that could include: inclinometers, tiltmeters, extensometers, time domain reflectometry, crackmeters, piezometers, among others. Complete monitoring systems have been seldom implemented and mostly for research purposes. In practical engineering, the restricted project budget limits the monitoring program to few instruments; thus, the correct location of the equipment on and in the slope is essential for obtaining adequate information that represents the complete mass performance. The location of instruments for slope stability is far from trivial. However, when a priori critical zones are identified such as geo-structural discontinuities, joints, faults, and so on, the instrumentation location is straightforward. Instruments should be placed where structurally weak zones, most heavily loaded zones, or zones where the highest pore water pressures are anticipated (Dunnicliff, 1993). In cases where no such critical zones are identified the selected location should reflect the behaviour of the whole body.

[1] PhD Student, Department of Civil Engineering, Structural Mechanics, KULeuven, Belgium, Email: jaime.bojorque@bwk.kuleuven.be
[2] Professor, Department of Civil Engineering, Structural Mechanics, KULeuven, Belgium, Email: guido.deroeck@bwk.kuleuven.be
[3] Professor, Department of Civil Engineering, Material Engineering, KULeuven, Belgium, Email: jan.maertens@bwk.kuleuven.be

The performance of slope stability modelling depends on the adequacy of obtaining quality data from monitoring. Whereas, the successful performance of monitoring depends on the ability to judge the optimal positioning of instruments. The information gathered from monitoring systems is needed to perform adequate slope maintenance, to perform repair measures, and to activate alarm-systems. The data obtained from monitoring is required to define or to adjust slope stability models through an interactive procedure. In addition, the selection of instrument locations should reproduce expected performance and should be compatible with the type of analysis that will be used when interpreting the data (e.g. Dunnicliff, 1993; Turner and Schuster, 1996). Geotechnical and Earthquake Engineering deal with uncertainties, therefore, adequate location of sensors (e.g. inclinometers, accelerometers), will reduce some uncertainties decreasing the lack of knowledge of the phenomenon involving a mass movement or a seismic event.

For most of the potential unstable slopes, the cost of prevention is less than the cost of remediation, as a result, if proper investigation is performed, the potential failure can be predicted saving human lives and avoiding expensive repairs (Simons et al., 2002). Finite element analyses support in identifying critical locations and preferred instrument orientations. The amount of information obtained from continuous monitoring in time and space makes numerical techniques ideal for managing this type of data. Numerical techniques have also demonstrated some advantages over traditional limit equilibrium methods and have shown that give similar results, i.e. factors of safety and slipping surfaces. Some comparative studies highlight the advantages of using numerical methods (e.g. Matsui and San, 1992; Griffiths and Lane, 1999; Dawson and Drescher, 1999).

In this research, optimization of sensor location from detecting the highest displacement in static, pseudo-static and dynamic slope stability analyses using finite element methods is proposed. This methodology is implemented in a potential landslide at km 27 along the Cuenca-Machala road, Ecuador. This paper focuses in the location of mass movement sensors by observing the static and dynamic performance of the slope. It is important to monitoring cut and slopes for detecting movements, and in the same hand, being aware about the importance of installing seismic instruments to better understand the seismic phenomenon of the zone.

GENERAL DESCRIPTION

Based on climate, lithological, earthquake activity, and topography information, Nadim et al., 2006, identified areas with the highest landslides and avalanches risk. In South-America, Ecuador, Colombia and Peru, have been identified as landslide high-risk geographic region, highlighting the importance of this description for planning programs. In the same study, Ecuador is classified as very high earthquake hazard zone. In Ecuador, the main landslide-risk areas are the roads that connect the highland cities on the Andes Mountains with the cities located on the coastal plain and the Amazon region. These roads cross through the steep slopes, weathered material, high precipitations zones, causing various instability problems. This region is also affected by continuous earthquake events of the Andean range.

In 2000 the Ministry of Public Work and Communications MOP-Ecuador contracted the studies of rehabilitation, improvement, expansion, maintenance, environmental impact, and economic and financial evaluation, on the Cuenca-Pasaje-Machala highway (MOP, 2002). This road is the main artery that connects Cuenca, the third most import city in Ecuador, and Machala located at the sea level. The road passes through the very steep Andean mountain range. Its altitude goes from about 2500 m a.s.l. at Cuenca to about 2760 m a.s.l. and then decreases steeply to Pasaje. The length of the road is about 154 km. Along the roadway 25 potential slope instabilities were identified. The instability problems identified are classified as: slides, rockfalls, debris flows, cut erosion, and settlements. In Figure 1 the location of the road within Ecuador is depicted.

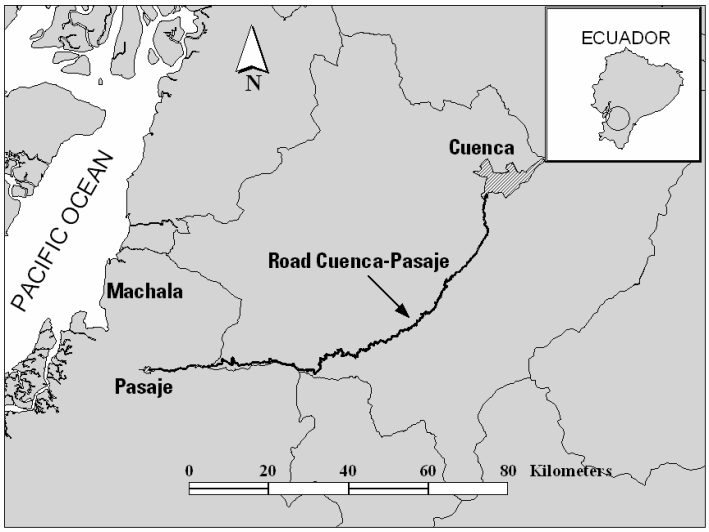

Figure 1. Project location, highway Cuenca-Pasaje

The potential landslide located between the abscissa km 27.620 and km 27.780 at the left hand side of the road is used as case study. It has a cut slope of about 40^{o} with a length of 130 m and it is 100 m wide, giving an approximated landslide volume of 240,000 m^3 with an average depth of 18.5 m. The presence of water increases the weathering which produces higher instability. This process is heightened from December to May which corresponds to the zone rainy period. The type of instability is described as active rotational slide in the cut slope located mainly on the superficial weathered material (MOP, 2002).

Geology and geotechnical characteristics

Three main lithological units were identified. First, the Colluvium which is toe and slope material deposits having undergone little transport. It is composed by heterogeneous mixtures of blocks and sub-angular to angular fragments, bounded by a clayey silty matrix. Secondly, the weathered tuff material which comes from the Saraguro formation, consisting of a reddish yellowish to white colour material, containing silty clay fines. Thirdly, The Saraguro formation underlying the previous units, it corresponds to the volcanic rock basement.

The depths of the layers were obtained from seismic refraction and electrical resistivity tests. Field values obtained from these tests were complemented with topographical and geological surveys. The basic geomechanical characteristics were obtained from soil classification, triaxial compression, and standard penetration tests. More details regarding the lithology composition and results of tests are given in the MOP, 2002 report. Table 1 summaries the geomechanical properties used for the analyses.

Table 1. Geomechanical properties

Parameter	Unit	Colluvium	Tuff	Rock
Natural unit weight (γ)	kN/m^3	16.67	17.64	24.50
Saturated unit weight (γ_{sat})	kN/m^3	19.17*	20.28*	24.50
Cohesion (c)	kPa	16.50	60.00	200.00
Friction angle (ϕ)	degrees	28.00	33.50	40.00
Young's modulus (E)	kPa	60	3000	6000
Poisson ration (v)	[-]	0.25	0.33	0.40

* γ_{sat} were considered 15% higher than γ

The field values obtained from seismic refraction and resistivity tests were related with the different strata. Table 2 presents the correlation between geology and geophysical tests.

Table 2. Correlation between Geology and Geophysical tests

Layer	Seismic Velocity (m/s)	Electrical Resistivity (ohm-m)	Thickness (m)	Material
1	161 – 646	9 – 18	2 – 22	Colluvium (material deposits)
2	1250 – 1928	2 – 16	22 – 51	Agglomeratic tuff slightly weathered
3	2500 – 3636	-	-	Volcanic basement rock (Saraguro Formation)

The seismic test values were used to derived the Young's modulus E[kPa] for the different strata, this computation was based on the compression wave velocity , Eq. 1(a & b), Kramer 1996.

$$V_p = \sqrt{\frac{G(2-2\nu)}{\rho(1-2\nu)}} \qquad \text{Eq. 1a}$$

solving for E with G=E/2(1+v) gives:

$$E = \frac{V_p^2 \gamma(1+\nu)(1-2\nu)}{g(1-\nu)} \qquad \text{Eq. 1b}$$

where, V_p= compression wave velocity [m/s], G= shear modulus [kPa], ν = Poisson's ratio [-], ρ = soil density [kg/m^3], γ = total unit weight [kN/m^3] and g is the gravity acceleration [9.8 m/s^2].

Model description

The Finite Element program PLAXIS (Finite Element Code for Soil and Rock Analysis) using 15-node elements and plane strain analysis, was selected. The soils were modelled as elastic-plastic material with Mohr-Coulomb yield criterion. Standard displacement boundary conditions, i.e. vertical and horizontal displacements restricted on the base and horizontal displacements on the sides, were implemented for the static model. Additionally of the static boundaries, absorbent boundary on the sides and prescribed displacement on the base for dynamic analyses were adopted. The stratigraphy, mesh discretization and boundary constraints are shown in Figure 2.

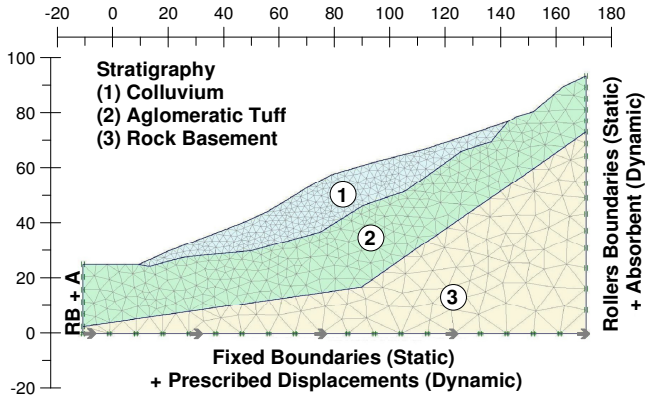

Figure 2. Model description

The initial state of stress for the slope was computed by the gravity loading procedure using the slope own-weight. For the static and pseudo-static analyses, the factors of safety (F_s) was computed by the shear strength reduction technique in which the cohesion and tanϕ are continuously decreased until non-convergence in the solution is obtained (phi/c reduction technique). The factor of safety is defined as the value by which the original shear strength parameters must be factored in order to bring the slope to failure. The same reduction factor was applied to both cohesion and tanϕ.

For the dynamic cases, the performance of the slope was based on the displacements generated by the ground motion record. The dynamic loading source was applied along the bottom of the model resulting to shear waves that propagate upwards. Material damping due to the viscous effects was taken into account via the Rayleigh damping. A damping coefficient (C) was assumed, which was proportional to the mass (M) and stiffness (K) of the system by $C = \alpha_1 M + \alpha_2 K$ where $\alpha_{1,2}$ represent the Rayleigh coefficients. Absorbent boundaries were used to ensure that an increase in stress on the boundary is absorbed without rebounding.

Selection ground motion record for dynamic analysis

There are three classical alternatives available to the engineer to obtain acceleration time-series (ground motion records), (i) artificial spectrum-compatible accelerograms, (ii) synthetic accelerograms generated from seismological source models taking into consideration the path and site effects, (iii) real accelerograms records (Bommer and Acevedo, 2004). Whit the increasing of earthquake recorded data, the use of real accelerograms has become more attractive, avoiding some drawbacks in the other methods. Real strong motion datasets are easily available for many parts of the world (e.g. Europe, Unite States, Japan, among others), however, for others, the lack of seismological data is noticeable. The selection of a real earthquake record to be used in the dynamic analysis is affected by the information available to the engineer regarding the seismic hazard or the design ground motion at the site of interest (Bommer and Acevedo, 2004). The selection of strong ground motion record, is usually selected based on the three parameters; magnitude, distance from the source to the site, and site characteristics. It is worth mentioning, that the magnitude strongly affect the shape of the response spectrum, thus, the selection of the record.

The ground motion record is based on the dataset available in Internet for South America, due to the lack of ground motion design code for the research zone. The Peru-Japan center for earthquake engineering research and disaster mitigation (CISMID) provides an alternative to obtain strong ground motion for the region. The accelerometer corresponded to the earthquake in 1966, recorded at the station Parque de la Reserva (PRQ). The component E-W, with a higher peak acceleration of 269.34 cm/sec^2 (0.275g) was used. The selection was based on the site characteristics and on the peak ground acceleration close to 0.25g and Magnitude 6.5. The basic PRQ-1966 earthquake characteristics are listed in Table 3 and in Figure 3 the recorded accelerogram, velocity, and displacement are shown.

Table 3. Earthquake PRQ-1966

Recording Site	Epicentral Location (Degrees)	Date (time)	Peak Acceleration (cm/sec^2)	Ms	Focal Depth (km)	Soil Condition
PRQ Parque de la Reserva, Peru	10.83° S 78.65° W	17/10/1966 (16:41)	-269.336 (0.275 g)	6.4	37.30	rock

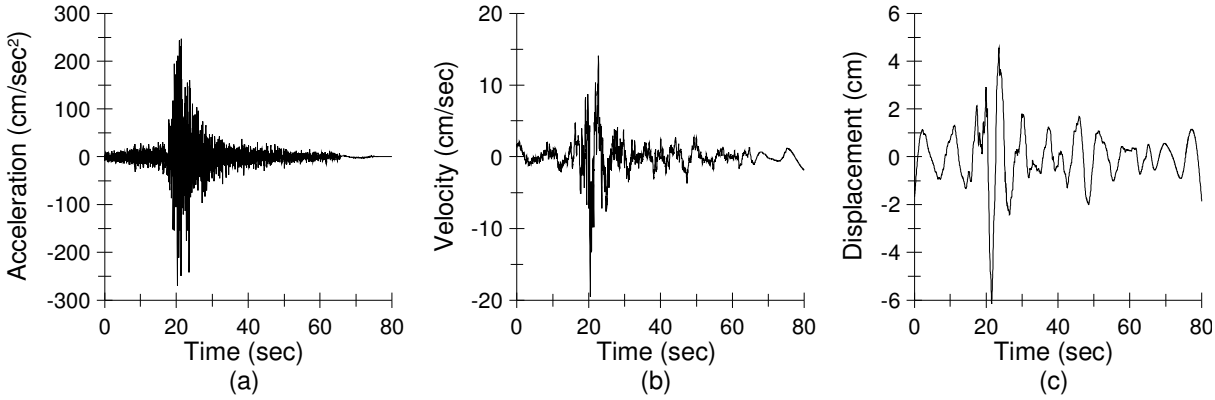

Figure 3. Parque de la Reserva PRQ-1966 earthquake
(a) acceleration, (b) velocity, (c) displacements

Validate record

To validate the performance of the selected record, the expected displacements obtained form performing Newmark (1965) rigid body procedure was used. Use was made of the JAVA code to compute Newmark's method developed by Jibson, R.W. and Jibson M.W, 2003. This method uses the critical seismic coefficient (k_c) as input parameter in order to derive the expected displacement. The k_c value is defined as the horizontal inertial force needed to be applied in the mass to obtain a factor of safety (F_s) equal to unity. In the framework of finite element method, k_c was obtained by gradually increasing the horizontal acceleration force until non-convergence in the finite element solution was achieved. After this load-increment the factor of safety was computed by the phi-c reduction technique, in which, the shear strength parameter were step by step decreased until non-convergence in the solution was reached. The factor of safety computed for that situation was lower than one. A new load-increment corresponding to 80% of the latter k_c-non-convergence value was imposed and then a new phi-c reduction was performed. For this case, a factor of safety near to unity will be obtained. To define the critical seismic coefficient which corresponds to F_s=1, a linear interpolation between these two previous F_s values was performed. This methodology has demonstrated to give similar k_c values as traditional pseudo-static limit equilibrium methods and log-spiral limit analysis. The k_c values for the original and final configuration (regraded slope) were 0.135 and 0.213 respectively.

Newmark's displacements were obtained by using the Earthquake PRQ-1966 record scaled to 0.25g, and for different k_c values; 0.05 ,0.075, 0.10, 0.135, 0.15, and 0.215 (Fig. 4). The displacements were 0.50 cm and 0.01 cm for k_c values of 0.135 and 0.213, respectively. The same procedure was used for 14 ground motion records available in the Jibson's interface. The records used in the analysis correspond to selected records that had a peak ground acceleration (PGA) between 0.20 and 0.30, and hard soil. All the selected records were scaled to 0.25g. The Newmark's displacement results are shown in Figure 4.

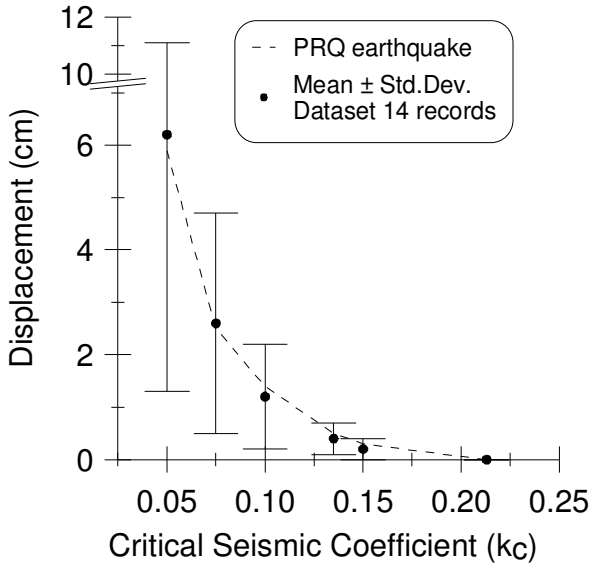

Figure 4. Newmark displacement

It can be appreciated that the PRQ-1966 results correspond to the mean value of all the records. It is worth noticing that when the critical seismic coefficient decreases the standard deviation of the displacements increases. Which implies that higher uncertainty in the analysis is introduced when k_c decreases.

SLOPE STABILITY ANALYSIS

Scenarios

Different scenarios were analyzed from which the locations of monitoring sensors could be selected. The scenarios differed by the incorporation of: groundwater, dynamic forces and/or remedial measures such as regrading of the slope and/or drainage system. Table 4 lists the different scenarios analyzed and the factors involved for each case. For scenarios 1, 3, and 6 to 9, groundwater was ignored by locating the water table at the bottom of the profile, i.e. zero pore pressure in the slope. For the others scenarios, the pore-water pressure variation was assumed to be hydrostatic and it was computed by multiplying the water table depth (z) by the water unit weight (γ_w) i.e., $u= \gamma_w z$. For these cases, the water table level on the left hand side was kept one meter below ground level, at 26 m. Meanwhile, in the right side it was fixed at 85 m. For the regrading of the slope, a 1V:2H (Vertical:Horizontal) slope with a middle terrace of 10 m wide at 20 m high from the toe was selected. The regarded configuration was considered in scenarios 3 to 5, 7 and 9. The incorporation of the drainage system was evaluated in scenario 5.

Table 4. Scenarios

Scenario #	Factor involved				Factor of Safety
	Water	Regrading	Drainage	Seismic	
1	No	No	No	No	1.39
2	*Yes*	No	No	No	0.99
3	No	*Yes*	No	No	1.65
4	*Yes*	*Yes*	No	No	1.05
5	*Yes*	*Yes*	*Yes*	No	1.31
6	No	No	No	*Yes-Pseudo*	See (Fig. 10)
7	No	*Yes*	No	*Yes-Pseudo*	See (Fig. 10)
8	No	No	No	*Yes*	---
9	No	*Yes*	No	*Yes*	---

For scenarios 6 and 7, dynamic forces were analyzed by a pseudo-static procedure applying a constant horizontal acceleration (a_h) as a fraction of the gravity. Even though, the recommend design a_h for this region is 0.2 to 0.25g (MOP-2002), for the initial configuration and values greater than 0.15g no plastic solution could be found, i.e. no stress distribution could be found that simultaneously satisfy both the Mohr-Coulomb failure criterion and global equilibrium. The performance of the slope by the effects of real earthquake motion record was analyzed in scenarios 8 and 9, for the initial and regarded configuration, respectively. The PRQ-1966 earthquake record was used for these computations. The location of the groundwater table considered for scenarios 2 and 5 and the configuration used for the regrading of the slope, cases 3-5, 7 and 9, are shown in Figure 5.

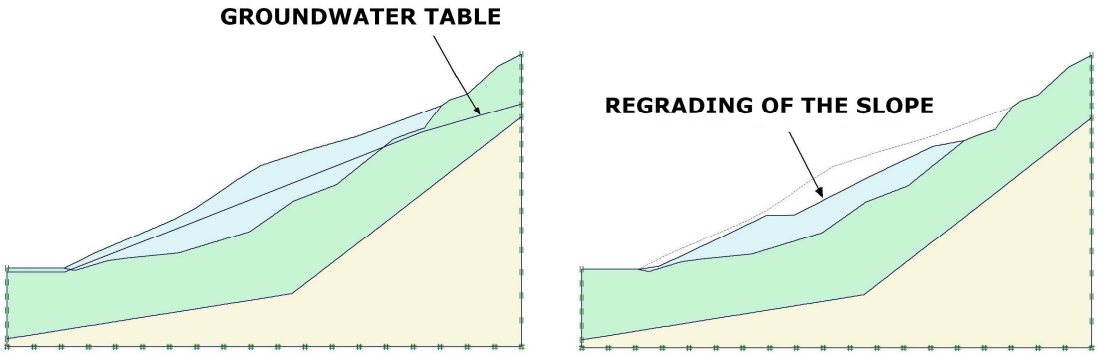

Figure 5. Groundwater and regrading configuration

Location of the highest displacements

In order to correct place the monitoring sensors, it is important to determine the locations where the highest displacements (strains) are generated within the slope. This detection has to be performed before failure has been produced. Indication of possible failure is essential to perform remedial measures for stabilization and/or activate alarm-systems. As a consequence a detail study on the zones where the highest displacements are located is required. The best location to place monitoring sensors was selected from determining the highest displacements i.e. horizontal, vertical, and total.

Static analyses, scenarios 1 to 5

In this section, the static slope stability is considered. Figure 6 shows the location where the highest displacements are generated for the initial configuration scenario 1. These displacements are computed from the displacement field obtained after performing a phi/c reduction procedure. The factor of safety obtained by FE, for scenario 1, was F_s=1.39. Within the slope the location of the Highest Horizontal (HHD), Vertical (HVD), and Total (HTD) Displacements all differ. The HHD are located on the colluviums' lower part at the left (Fig. 6a), whereas the HTD are placed on the right of the slip surface (Fig. 6c). The HVD are located near to the ground at the upper part of the slip surface (Fig. 6b). It is worth mentioning that, the critical locations of the HVD, which are located near the surface, remain almost the same along the phi/c reduction procedure. In consequence, the location of the HVD, gives a good position for installing instruments which are appropriated to detect vertical movements.

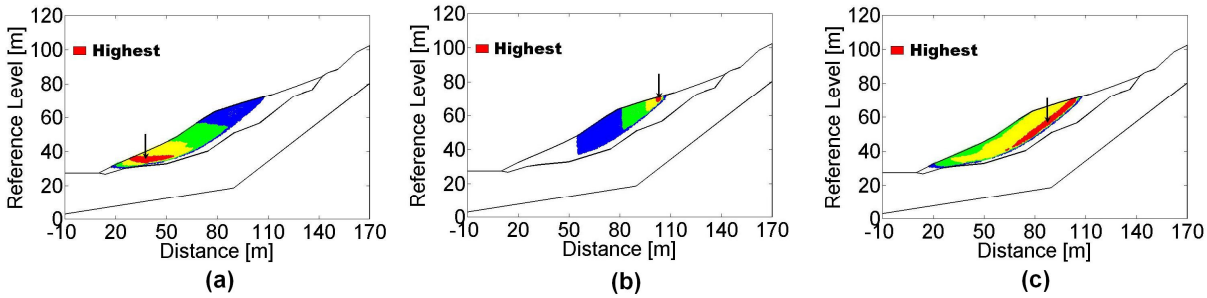

Figure 6. Highest displacement for the initial configuration, scenario 1 (a) Horizontal HHD, (b) Vertical HVD, and (c) Total HTD

Plots of HTD for scenarios 2 to 4 are shown in Figure 7. In the initial configuration, a shifting in the location of the HTD is produced when groundwater is considered. The HTD for scenario 2 are situated at the left hand side in the lower part of the colluvium (Fig. 7a). The influence of the groundwater is clear by decreasing the F_s to a value equal to 0.99. Therefore, in this condition the slope is unstable. The regraded slope, case 3, reveals a sliding mechanism located at the right upper part of the colluvium layer. The volume of sliding mass decreased and it is located in the upper slope. By performing the grading of the slope the F_s rose to 1.65. For the regraded slope, Figure 7b displays the slip surface and the location where the HTD developed at the last step, scenario 3. If groundwater is considered in the regraded slope, scenario 4, the failure mass extends to the entire colluvium strata. And the locations of the HTD are placed in the ground at the middle of the second terrace. Moreover, when groundwater is considered in the regraded configuration, the slope is near to failure with a F_s equal to 1.05. The sliding surface and the location of the HTD for scenario 4 is shown in Figure 7c. To increase the stability a drainage system, which reduces the groundwater level in the colluvium, was analyzed in scenario 5. This drainage scenario rose the F_s to 1.31. Further details on the slope-static performance can be found else where (Bojorque et al., 2006).

Pseudo-static analyses, scenarios 6 and 7

The influence of dynamic forces on the slope stability is considered by two methods. First, by considering the dynamic force as a constant horizontal acceleration i.e. pseudo-static analysis. Secondly, by performing a dynamic finite element analysis.

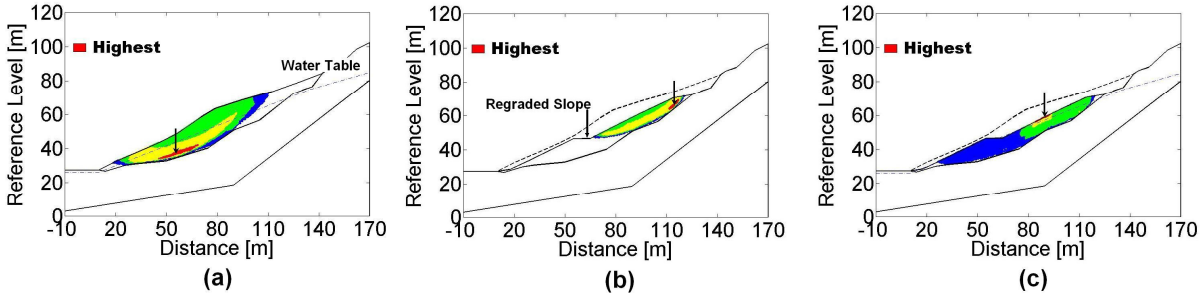

Figure 7. Highest Total Displacement (HTD)
(a) scenario 2 [Groundwater], (b) scenario 3 [Regraded], and (c) scenario 4 [Regraded + GW]

The pseudo-static and dynamic analysis are implemented for the initial configuration cases 6 and 8, and regraded slope cases 7 and 9, respectively. When the seismic force by pseudo-static analysis is considered, cases 6 and 7, and after performing a phi/c reduction, the locations where the HTD, HHD, and HVD occur remain equal to scenario 1 and 3, respectively. Figure 8 shows the location of the highest displacements for the regraded slope, scenario 7, after applying a value of a_h=0.2g.

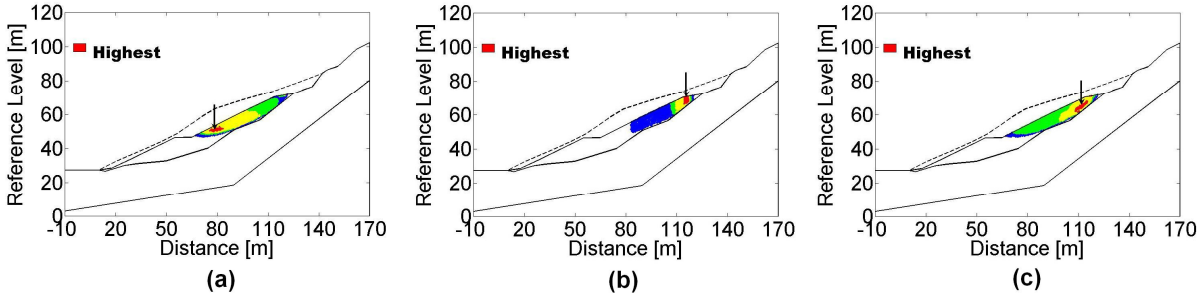

Figure 8. Highest displacement for pseudo-static a_h=0.20g, scenario 7
(a) Horizontal HHD, (b) Vertical HVD, and (c) Total HTD

Figure 9 shows the HHD developed for different horizontal acceleration for the initial situation, scenario 6. The displacement field used to compute the highest displacements corresponded to those obtained after applying a_h. The corresponding factor of safety computed by the phi/c reduction procedure are given together with the input a_h.

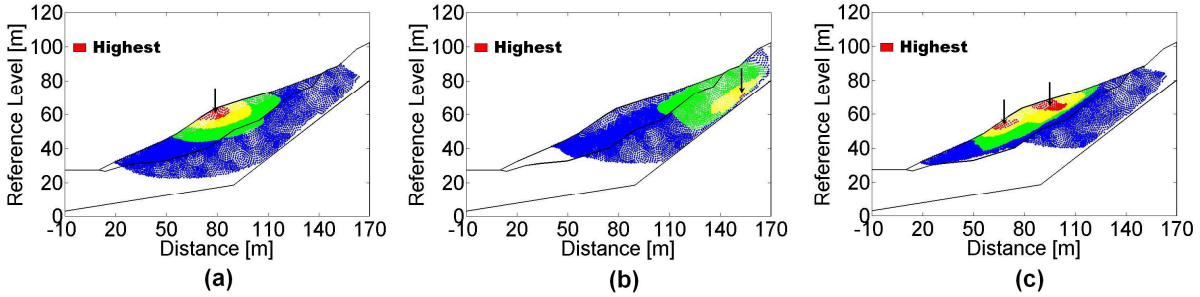

Figure 9. Highest Horizontal Displacement (HHD), scenario 6
(a) 0.0055g [F_s=1.37], (b) 0.1170g [F_s=1.05], and (c) 0.1455g [F_s=0.98]

The HHD shifted from the colluvium to the tuff when the a_h value increases. The same behaviour is produced for the regraded slope, scenario 7. A relationship between the horizontal acceleration (a_h) and the factor of safety (F_s) is obtained for the initial and regraded configuration. The trend is a straight line with a slope of 2.8 for the regraded slope and 3 for the initial configuration. Figure 10 shows the correlation between the factor of safety and horizontal acceleration in the pseudo-static analysis for the initial and regraded configurations. The goodness of fit for the linear trend in both cases is very high.

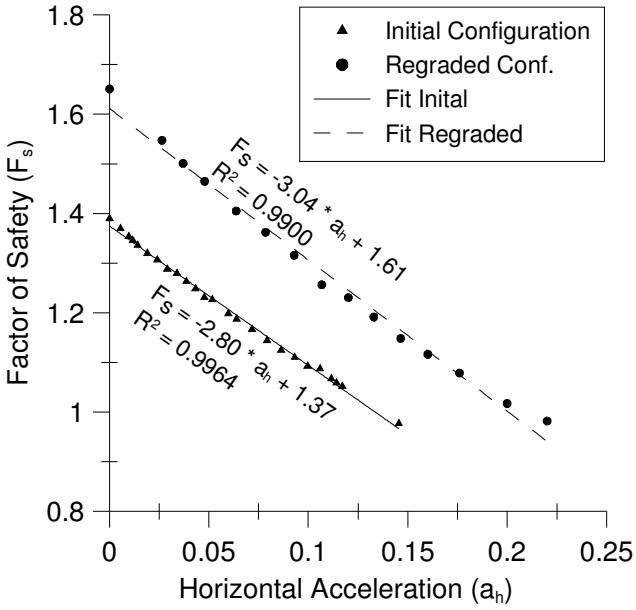

Figure 10. Factor of safety vs. Horizontal acceleration coefficient

Dynamic analyses Scenarios 8 and 9

The influence of dynamic forces produced by the PRQ-1966 earthquake is considered. Figure 11 shows the location of the highest displacements developed after applying both the earthquake acceleration record and phi/c reduction procedure. The HHD shifted from the left side of the sliding surface to the centre and then returns to the left side. Meanwhile the HVD remain located in the upper part of the colluvium at ground level. The HTD shifted from the right side to the centre of the slope.

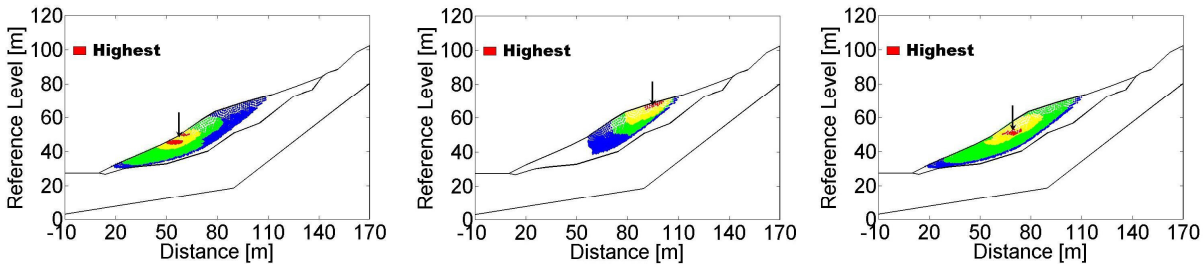

Figure 11. Highest displacement for the initial configuration, scenario 8
(a) Horizontal HHD, (b) Vertical HVD, and (c) Total HTD

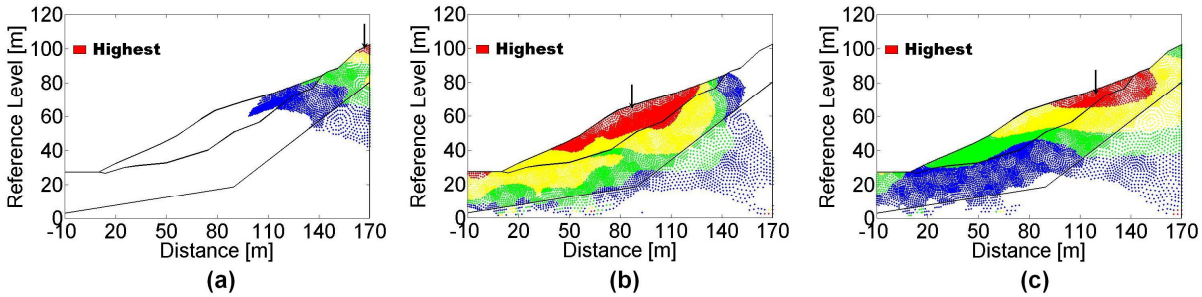

Figure 12. Highest horizontal displacement (HHD), scenario 8
(a) -0.0001g, (b) 0.0001g, and (c) 0.0031g

Figure 12 shows the relative displacements field computed for scenario 8 for three different earthquake acceleration; -0.0001g, 0.0001g, and 0.0031g. The relative displacements are computed with respect the bottom of the model, where the earthquake was input by prescribed displacement

conditions. The highest relative displacements are developed at the upper part of the profile. The same behaviour is presented for the regraded slope, scenario 9, where the highest relative displacements are located in the upper part of the model. No clear location of sensor could be judge from this performance, however, ground sensor located in the upper colluvium could help to identify slope movements. A phi/c reduction procedure was applied to different stress fields computed from applying the earthquake force. The location of the highest displacements after the phi/c reduction remain equal for all the forces and are similar to Fig. 11. Figure 13 shows the variation of the factor of safety by incorporating the PRQ-1966 earthquake. No clear tendency in the computed factor of safety could be detected. However, under the PRQ-1966 ground motion the slope is stable.

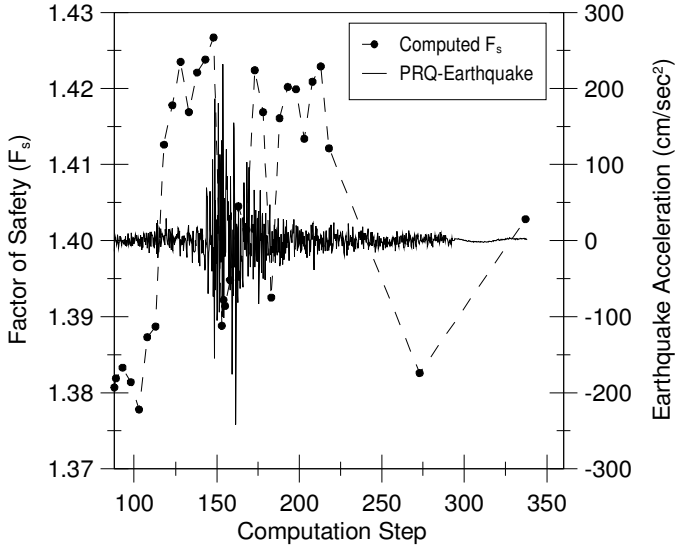

Figure 13. Factor of safety for different earthquake acceleration

CONCLUSIONS AND FUTURE WORK

The best location to install field sensor for landslide monitoring were selected based on static, pseudo-static and dynamic finite element slope stability analysis. The potential unstable slope at km 27 along the Cuenca-Machala highway in Ecuador was analyzed. From the analysis, it is suggested that, horizontal displacement sensor should be located in the toe of the slope where the highest horizontal displacements HHD were generated. Based on the static and pseudo-static analyses the best location to install vertical displacement is the upper part of the colluvium. It should be noted that the HVD remain for the different scenarios. The advantages for these locations are that they were produced in the ground surface, thus the installation of sensor is more convenient. In the other hand, the total displacements, for most of the cases, were located where the sliding surface was generated. To detect these HTD boreholes should be constructed and inclinometers should be installed. When groundwater was considered the HTD were developed in the contact zone between the colluvium and the tuff material. The slope was in marginal stability when groundwater was incorporated. Stability can be improved by regrading the slope and installing a subdrainage system to facilitate water flows. Monitoring the performance of drainage systems is very important to limit the groundwater to rise in the slope. Groundwater measurements should be located in the upper colluvium.

In the pseudo-static analysis, when looking through the displacement filed calculated from increasing of the horizontal acceleration coefficient, the location where the highest displacements were generated changes. However, for all the cases after performing a phi/c reduction on the stress field computed with different a_h, the locations where the highest displacements were generated remained equal to the static ones. The assumption of constant horizontal acceleration acting in the whole slope should be used carefully. Besides, the displacements pattern, a clear linear trend is computed for the relationship between the factor of safety and the horizontal acceleration coefficient.

The application of the PRQ-earthquake produced a small shift in the location of the HHD. The location of the horizontal displacements moved upwards to the middle of the slope. Meanwhile, the HTD moved from the lower part of the sliding surface to the ground. The HVD, as for the static cases, remained in the upper colluvium ground. No clear tendency of the location of the highest displacements was detected from the displacement field computed for each acceleration time step (ground motion record). The PRQ-earthquake record produced slightly changes in the factor of safety, without compromising the slope stability. However, the serviceability should be check to guarantee the performance of adjacent structures. The influence of the earthquake pattern (magnitude and frequency), soil amplification, and uncertainties in soil parameters, on the location of the highest displacements will be considered in further studies.

AKNOWLEDGEMENTS

The first author would like to thank for the financial support provided by the K.U.Leuven in the context of the Selective Bilateral Agreement between K.U.Leuven and Latin-America.

REFERENCES

Bojorque J., De Roeck G., and Maertens J., "The use of finite element analysis in monitoring landslides". Proc. 7th National Congress on theoretical and applied Mechanics NCTAM, Mons, Belgium, 2006.

Bommer J.J., and Acevedo A.B., "The use of real earthquake accelerograms as input to dynamic analysis". *Journal of Earthquake Engineering* 8(Special Issue 1), 43-91, 2004.

CISMID, The Peru-Japan center for earthquake engineering research and disaster mitigation [online], http://www.cismid-uni.org/, Retrieved 2006.

Dawson E. and Drescher W., "Slope Stability Analysis by Strength Reduction", *Geotechnique*, 49(6), 835-840, 1999.

Dunnicliff J., *Geotechnical Instrumentation for Monitoring Field Performance*, John Wiley and Sons, Inc., 1993.

Griffiths D. and Lane P., "Slope Stability Analysis by Finite Elements", *Geotechnique*, 49(3), 387-403, 1999.

Jibson R.W. and Jibson M.W., "Java programs for using Newmark's method and simplified decoupled analysis to model slope performance during earthquakes". Version 1.0. Denver, Colorado, U.S. Geological Survey, Open-file report 03-005-2003

Kramer S.L., *Geotechnical Earthquake Engineering*, Prentice Hall, Inc., Upper Saddle River, New Jersey, 653 pp., 2006.

Matsui T. and San K-C., "Finite Element Slope Stability Analysis by Shear Strength Reduction Technique", *Soils and Foundations*, 32(1), 59-70, 1992.

MOP, Ministerio de Obras Publicas y Comunicaciones, Ecuador. "Estudios de Rehabilitación, Ampliación, Mantenimiento, Impacto Ambiental y Evaluación para la Concesión de la Carretera Cuenca-Machala"., Reporte Interno, Ecuador, 2002.

Nadim F., Kjekstad O., Peduzzi P., Herold C., and Jaedicke C., "Global landslide and avalanche hotspots". *Landslides,* 3, 159–173, 2006.

Newmark N., " Effects of earthquakes on dams and embankments ". *Geotechnique* 15 (2), 139-160, 1965.

PLAXIS, "Finite Element Code for Soil and Rock Analysis", 2D-Version 8, Slope Stability Analysis, Delft University of Technology and Plaxis, The Nederlands, 2004.

Simons N., Menzies B., and Matthews M., *A short course in Geotechnical Site Investigation*, Thomas Telford, 2002.

Turner A.K. and Schuster R.L., *Landslides. Investigation and Mitigation*, Special Report 247. Transportation Research Board. National Research Council. Washington DC. 673 p., 1996.